Dynamic Response of Dye-Sensitized Nanocrystalline Solar Cells: Characterization by Intensity-Modulated Photocurrent Spectroscopy

L. Dloczik,[†] O. Ileperuma,[‡] I. Lauermann,[†] L. M. Peter,*[,§] E. A. Ponomarev,[||] G. Redmond,[§] N. J. Shaw,[§] and I. Uhlendorf[†]

Institut für Angewandte Photovoltaik, Munscheidstrasse 14, D-45886 Gelsenkirchen, Germany, Department of Chemistry, University of Peradeniya, Sri Lanka, School of Chemistry, University of Bath, Bath BA2 7AY, U.K., and Laboratoire de Physique des Solides de Bellevue, CNRS, UPR 1332, 1 Place Aristide Briand, 92195 Meudon, France

Received: July 28, 1997; In Final Form: October 8, 1997[⊗]

The frequency-dependent photocurrent response of dye-sensitized TiO_2 cells to modulated illumination is analyzed. Analytical expressions are derived that describe generation, collection, and recombination of electrons in a thin layer nanocrystalline solar cell under conditions of steady illumination and with a superimposed small amplitude modulation. The analysis considers illumination from the contact side and from the counter electrode side, and characteristic differences in the intensity-modulated photocurrent response are predicted for the two cases. The attenuation of the ac photocurrent by the *RC* time constant of the cell is also considered. The theoretical analysis shows that intensity modulated photocurrent spectroscopy (IMPS) can provide new insight into the dynamics of electron transport and collection in the dye-sensitized solar cell. Experimental IMPS data measured for high-efficiency dye-sensitized cells are fitted to the theoretical model using Bode plots in order to derive values of the lifetime (2×10^{-2} s) and diffusion coefficient (5×10^{-5} cm^2 s^{-1}) of photoinjected electrons.

Introduction

Dye-sensitized nanocrystalline solar cells with AM 1.5 efficiencies of up to 10% have been developed by Grätzel and co-workers.[1−3] The devices rely on injection of electrons from a photoexcited ruthenium dye into the nanocrystalline TiO_2 phase followed by collection at the contact electrode, usually tin oxide coated glass. Since the particle size in the nanocrystalline phase is small and the electrolyte phase penetrates throughout the porous solid phase, the contribution of internal electrical fields to carrier collection in the TiO_2 phase is expected to be negligible. Electron transport must therefore involve diffusion coupled to relaxation of the ionic atmosphere in the electrolyte phase. This intimate coupling between the two phases represents a novel physical situation that contrasts with the collection of minority carriers in conventional p−n or Schottky barrier solar cells, where the electric field in the depletion layer assists carrier separation, and diffusion is restricted to the quasi-neutral region. Electron diffusion in the nanocrystalline oxide phase is evidently slow (as we shall see, typical transit times are 10 ms or more), so that it is essential for the success of the dye-sensitized cell that back-reaction of electrons in the TiO_2 and in the highly doped tin oxide coated glass substrate with I_3^- is sufficiently slow that electrons injected by the photoexcited dye are collected efficiently. Clearly, characterization of carrier transport, trapping, and recombination in nanocrystalline cells is a major challenge, and this paper shows that intensity-modulated photocurrent spectroscopy (IMPS) offers new insights into these processes.

The steady-state $i-V$ response of dye-sensitized nanocrystalline cells has been discussed by Södergren et al.,[4] who give steady-state solutions of the generation/collection equation for the density of mobile excess electrons

$$\frac{\partial n}{\partial t} = D\frac{\partial^2 n}{\partial x^2} - \frac{n}{\tau} + \alpha I_0 e^{-\alpha x} \qquad (1)$$

for illumination from the contact and counter electrode sides. Here D is the diffusion coefficient of electrons and τ is the electron lifetime determined by back-reaction with I_3^-. This process is commonly referred to as recombination, and its rate is assumed to be first order in electron density, although it may not be first order in I_3^-.[5] I_0 is the incident photon flux corrected for reflection losses, and α is the absorption coefficient. α is determined by the extinction coefficient of the dye, the internal surface area, the fractional surface coverage of the dye, and light scattering. Light absorption by I_3^- is neglected. The generation term in eq 1 implies that the electron injection efficiency is unity, but as O'Regan et al.[6] have shown, the rate of back-reaction of electrons with the oxidized state of the dye is potential dependent, and close to open circuit, regeneration of the dye by reaction of its oxidized state with I^- may no longer suppress this recombination route. In this case, the quantum efficiency for electron generation will be less than unity.

The expressions obtained by solving eq 1 can be reduced to forms that resemble the conventional diode equation for a solid-state photovoltaic device.[4].

$$j = j_{\text{photo}} - j_0(1 - e^{(qV)/(mkT)}) \qquad (2)$$

where j_{photo} is the photocurrent, j_0 is the saturation dark current under reverse bias, V is the voltage, and m is a nonideality factor that is reported to be close to 2 for the dye-sensitized cell.[4,5] The open circuit photovoltage $V_{\text{photo}} = V_{\text{oc}}$ is defined by the condition $j = 0$.

Equation 1 has been solved numerically by Cao et al.[7] for conditions of periodic and pulsed illumination from the counter electrode side, but although the solutions reproduce the gross

* Corresponding author. Email: l.m.peter@bath.ac.uk.
[†] Institut fü Angewandte Photovoltaik.
[‡] University of Peradeniya.
[§] University of Bath.
[||] CNRS.
[⊗] Abstract published in *Advance ACS Abstracts,* November 15, 1997.

S1089-5647(97)02466-8 CCC: $14.00

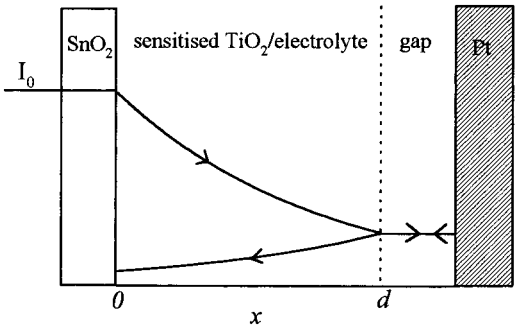

Figure 1. Geometry for illumination of the dye-sensitized cell from the substrate side, showing the contribution due to reflection from the platinum electrode. In some experiments, the platinum electrode was replaced by a transparent electrode to allow illumination from the electrolyte side.

features of the experimental results, they are not convenient for comparison with experimental data. These authors also consider the case where the diffusion coefficient of electrons in the nanocrystalline phase depends on light intensity as the result of the occupancy of electron traps. In related work, De Jongh and Vanmaekelbergh have discussed the transport of electrons generated by band-gap illumination of nanocrystalline TiO_2[8,9] and have predicted the IMPS response for the case where the penetration depth of the light is much smaller than the film thickness. These authors also consider the effects of electron trapping. However, up to now no convenient *general* analytical solutions have been available that can be used routinely to analyze IMPS data.

The treatments mentioned above assume that electron extraction at the substrate is diffusion controlled. By contrast, the present paper takes a more general approach. The junction between the nanocrystalline oxide and the conducting substrate is not well understood, but it can be pictured as an array of point contacts to TiO_2 nanoparticles. The contact is complicated by the fact that the electrolyte phase also penetrates to the back of the porous layer. We therefore consider that electron extraction across the TiO_2/SnO_2 junction may involve a non-negligible activation energy. Furthermore we consider that changes in the potential of the electrode may affect the activation energies for electron extraction and injection in a way analogous to conventional electrode kinetics or field assisted ionic transport in oxides.

This paper presents convenient analytical expressions for the steady state and IMPS responses and uses them to examine the influence of carrier lifetime, diffusion coefficient, and film thickness on the photocurrent response. The expressions include the rate constant for electron extraction at the substrate, and they are readily reduced to the expressions for diffusion-controlled extraction. The influence of the *RC* time constant of the cell on the IMPS response is also considered. The experimental IMPS response of high efficiency dye-sensitized TiO_2 cells has been measured, and the results have been fitted using the analytical expressions for the frequency dependent photocurrent response.

Theory

We consider the geometry shown in Figure 1. The thin film of nanocrystalline semiconductor (thickness d) is presumed to be uniformly sensitized with dye so that the absorption coefficient α is independent of distance. Light absorption by I_3^- in the pores is not considered, and light scattering by the nanocrystalline phase is treated semiempirically by defining an effective absorption coefficient. The electrolyte phase is assumed to penetrate throughout the porous film so that injected electrons are screened by counterions and solvent dipoles in the electrolyte. Coulombic interactions between injected electrons are assumed to be negligible. The lifetime of excess electrons in the nanocrystalline solid is presumed to be determined by back reactions with the oxidized component of the supersensitizer couple (I^-/I_3^-). Regeneration of the dye from its oxidized state by reaction with I^- is assumed to be fast compared with the time scale of the modulation. Depletion of I^- and accumulation of I_3^- in the pores of the film are neglected. The effects of electron trapping are considered and related to the effective diffusion coefficient of electrons, D_{eff}, determined by the expression

$$D_{\mathrm{eff}} = D\frac{n_{\mathrm{free}}}{n_{\mathrm{total}}} = D\frac{k_{\mathrm{detrap}}}{k_{\mathrm{trap}} + k_{\mathrm{detrap}}} \tag{3}$$

where n_{free} is the density of free conduction band electrons, n_{total} is the total density of free and trapped electrons, and k_{trap} and k_{detrap} are the first-order rate constants for trapping and detrapping of electrons. The possibility of electron recombination with I_3^- via trap states is also included. The influence of the *RC* time constant of the system is considered since impedance measurements show that electron accumulation at potentials near V_{oc} gives rise to capacitances exceeding 1 mF cm^{-2}. In fact, the experimental results show that the IMPS response is modified by the *RC* time constant even under short circuit conditions (Vanmaekelbergh et al.[10] have also discussed the effect of the *RC* time constant for porous GaP, where the space charge capacitance only becomes important close to flat-band).

The IMPS technique involves superimposing a small sinusoidal perturbation on a larger dc illumination level. The use of small (relative) modulation amplitudes has the advantage that the diffusion coefficient of electrons can be considered to be determined primarily by the dc illumination intensity. It has been observed that the diffusion coefficient of electrons in dye-sensitized nanocrystalline TiO_2 cells increases with light intensity, probably as the result of light-dependent trap filling.[8−11] An exact theoretical treatment in this case is complicated because the effective diffusion coefficient is not constant throughout the film since the local carrier generation rate depends on distance and the trap occupancy is determined by the quasi-Fermi level of electrons, which also varies with distance. The relaxation of trapped electrons may influence the IMPS response, and this situation is also discussed here. However, these complications need not obscure the fundamental properties of the dye-sensitized nanocrystalline cell.

Details of the derivation of the following expressions are given in the Appendix. We consider the general case where electrons diffuse to the back contact and are then extracted over a potential-dependent energy barrier with a characteristic potential dependent rate constant k_{ext}. The diffusion-limited case is obtained by letting k_{ext} become large (the analogy with conventional electrode kinetics is exact). On the other hand, when k_{ext} is small the kinetically (or recombination) limited case is obtained. We assume that injection of electrons from the degenerate SnO_2 substrate also occurs across the energy barrier with a potential (i.e., photovoltage) dependent rate constant k_{inj}. The rate constants for the forward and reverse reactions are given by

$$k_{\mathrm{ext}} = k_{\mathrm{ext}}^0 \exp\left[\frac{-q\beta V}{kT}\right] \tag{4a}$$

and

$$k_{inj} = k_{inj}^0 \exp\left[\frac{q(1-\beta)V}{kT}\right] \tag{4b}$$

where V is the cell voltage and β is analogous to the electrochemical transfer coefficient or symmetry factor and reflects the way in which changes in the potential at the TiO_2/substrate interface affect the rate constants for forward and reverse electron transfer.

For illumination from the electrolyte side, we find that the ac photocurrent conversion efficiency $\Phi(\omega) = j_{photo}/qI_0$ is given by

$$\Phi(\omega) = \frac{\alpha}{\alpha+\gamma} \cdot \frac{e^{(\gamma-\alpha)d} - e^{-(\alpha+\gamma)d} + 2\alpha\dfrac{e^{(\gamma-\alpha)d}-1}{\gamma-\alpha}}{e^{\gamma d} + e^{-\gamma d} + \dfrac{D\gamma}{k_{ext}}(e^{\gamma d} - e^{-\gamma d})} \tag{5}$$

where α is the effective absorption coefficient and d is the film thickness. γ is given by

$$\gamma = \sqrt{\left(\frac{1}{D\tau} + \frac{i\omega}{D}\right)} \tag{6}$$

The corresponding dc solutions are obtained by setting

$$\gamma = \sqrt{\left(\frac{1}{D\tau}\right)} \tag{7}$$

If k_{ext} becomes large, we obtain the diffusion-limited case, and eq 5 becomes

$$\Phi(\omega) = \frac{\alpha}{\alpha+\gamma} \cdot \frac{e^{(\gamma-\alpha)d} - e^{-(\alpha+\gamma)d} + 2\alpha\dfrac{e^{(\gamma-\alpha)d}-1}{\gamma-\alpha}}{e^{\gamma d} + e^{-\gamma d}} \tag{8}$$

For illumination from the substrate side, the general solution is

$$\Phi(\omega) = \frac{\alpha}{\alpha+\gamma} \cdot \frac{e^{\gamma d} - e^{-\gamma d} + 2\alpha\dfrac{e^{-\alpha d}-e^{-\gamma d}}{\gamma-\alpha}}{e^{\gamma d} + e^{-\gamma d} + \dfrac{D\gamma}{k_{ext}}(e^{\gamma d} - e^{-\gamma d})} \tag{9}$$

and the corresponding diffusion-controlled limit is given by

$$\Phi(\omega) = \frac{\alpha}{\alpha+\gamma} \cdot \frac{e^{\gamma d} - e^{-\gamma d} + 2\alpha\dfrac{e^{-\alpha d}-e^{-\gamma d}}{\gamma-\alpha}}{e^{\gamma d} + e^{-\gamma d}} \tag{10}$$

In the diffusion-controlled limit, the dc solutions obtained from eqs 8 and 10 by setting $\omega = 0$ are identical with those derived by Södergren et al.[4] The current voltage characteristics of the dye-sensitized cell can be derived from the preceding theoretical considerations. In particular, we note that the open circuit voltage is defined by $j_{photo} = j_{dark}$ where both j_{photo} and j_{dark} are determined by the solutions of the diffusion equation for electrons.

D and τ have been treated as a constants in the preceding expressions. If carrier relaxation from traps is fast compared to the modulation frequency and if recombination of trapped electrons is negligible, D can be replaced by an (intensity-dependent) effective diffusion coefficient, D_{eff}, defined by eq 3 (cf. Appendix). Similarly τ is replaced by the effective electron lifetime as described by eq A23. If carrier relaxation is slow, it may affect the periodic IMPS response. This case is also discussed in the Appendix, which gives an example of the predicted IMPS response. To address the main features of the IMPS response of nanocrystalline systems at this point, we restrict discussion to the cases where trapping does not influence the shape of the IMPS plots but is only manifest in the effective electron lifetime and effective diffusion coefficient (the conditions under which this approach is valid are defined in the Appendix). It should be noted that both D and τ may be voltage dependent, since they will depend on trap occupancy if trapping effects are important.

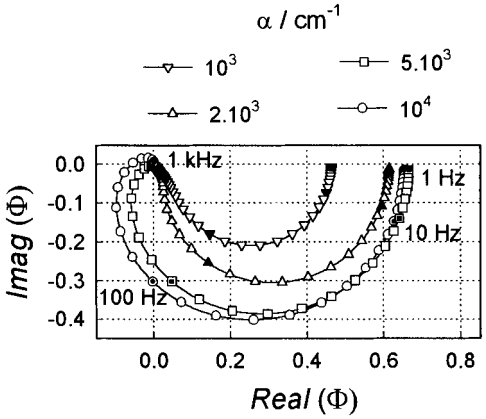

Figure 2. Calculated IMPS plots (diffusion-controlled limit) for illumination from the electrolyte side. Film thickness d 12 μm, electron lifetime τ 10^{-2} s, electron diffusion coefficient D 10^{-4} cm^2 s^{-1}, absorption coefficient α as shown. Note that for small light penetration depths, the IMPS response crosses the imaginary axis before tending to zero at high frequencies.

The expressions given above relate to the current generated internally in the dye-sensitized cell. The frequency dependent photocurrent measured in the external circuit is attenuated by the parallel combination of the electrode capacitance and the resistance of the electrodes and solution. In practice, the resistance is dominated by the sheet resistance of the tin oxide coated glass. In general, the measured IMPS response Φ_{ext} takes the form

$$\Phi_{ext}(\omega) = \Phi_{int}(\omega)\, A(\omega) \tag{11}$$

where

$$A(\omega) = \frac{1 - j\omega RC}{1 + \omega^2 R^2 C^2} \tag{12}$$

is the RC attenuation factor and Φ_{int} is the photocurrent conversion efficiency defined by eq 5 or eq 8.

The influences on the IMPS response of the illumination geometry, absorption coefficient, electron lifetime, rate constant for electron extraction and RC time constant are illustrated in Figures 2−7. The first thing to note is that the imaginary component of the IMPS response is negative under most conditions. This contrasts with the IMPS response for a minority carrier device, which has a positive imaginary component arising from the flux of majority carriers involved in recombination.[12] It can be seen from Figure 2 that the IMPS plot for illumination from the electrolyte side crosses into the negative real quadrant and the positive imaginary quadrant before tending to zero in the high-frequency limit. This behavior can be understood in terms of the diffusion-controlled transit time required for carriers generated at the outside of the film to reach the substrate. In the limit of very small penetration depth of the light, the IMPS signature spirals into the origin as predicted by Vanmaekelbergh et al.[10] By contrast, Figure 3

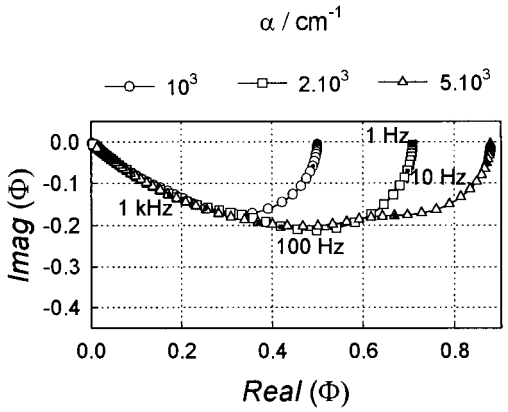

Figure 3. Calculated IMPS plots (diffusion-controlled limit) for illumination from the substrate side. Film thickness d 12 μm, electron lifetime τ 10^{-2} s, electron diffusion coefficient D 10^{-4} cm^2 s^{-1}, absorption coefficient α as shown. Note that in this case, the high-frequency response tends toward the 45° line characteristic of diffusion control.

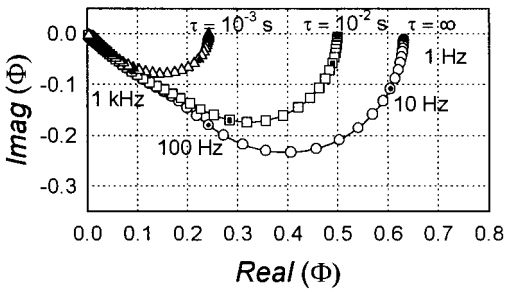

Figure 4. Calculated IMPS plots (diffusion-controlled extraction) illustrating the effect of the electron lifetime τ. Film thickness d 12 μm, electron lifetime τ 10^{-2} s, electron diffusion coefficient D 10^{-4} cm^2 s^{-1}, absorption coefficient α 10^3 cm^{-1}.

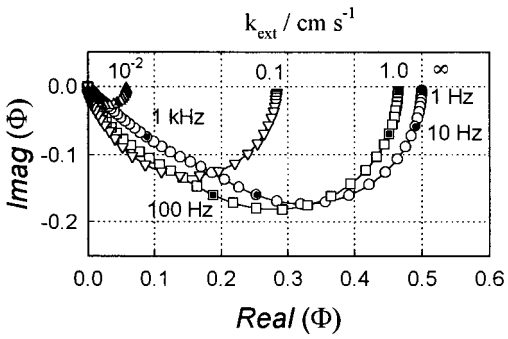

Figure 5. Calculated IMPS plots showing influence of kinetically limited electron extraction at the substrate contact. Film thickness d 12 μm, electron lifetime τ 10^{-2} s, electron diffusion coefficient D 10^{-4} cm^2 s^{-1}, absorption coefficient α 10^3 cm^{-1}, k_{ext} as shown. Note the transition to a semicircular IMPS response as k_{ext} is reduced.

shows that the IMPS signature for illumination from the substrate side remains in one quadrant, and at high frequencies, the plot tends toward the origin along a straight line with a slope of 45°. Practical cells utilize a reflective platinum secondary electrode to enhance regeneration kinetics and light harvesting,[3] and in this case the IMPS response is expected to be a scaled linear superposition of the shapes characteristic of the two illumination geometries.

The effect of the electron lifetime is illustrated in Figure 4. If the lifetime is sufficiently long, all photoinjected electrons are collected, and the dc value of Φ is determined by the fraction of incident light that is absorbed. For a finite electron lifetime, the dc photocurrent conversion efficiency depends on the ratio

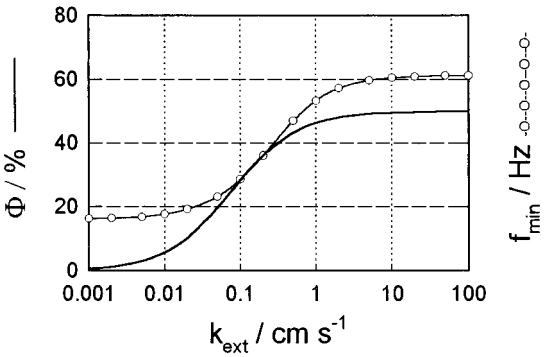

Figure 6. Plots showing dependence on k_{ext} of the dc photocurrent conversion efficiency Φ and of the frequency (Hz) corresponding to the minimum in the IMPS response. Note that the k_{ext} axis is equivalent to a voltage axis (cf. eq 4a). The limiting value of ω_{max} as k_{ext} becomes small is determined by the electron lifetime ($\omega_{max} = 1/\tau$).

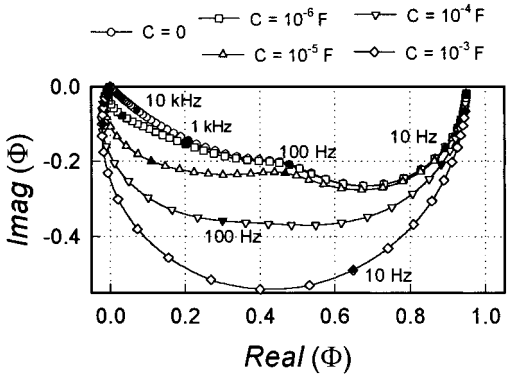

Figure 7. IMPS plots showing the influence of the *RC* time constant (diffusion-limited case). Illumination from the substrate side. R = 10 Ω, C as shown.

between the electron diffusion length $L = (D\tau)^{1/2}$ and the film thickness.

The theoretical treatment predicts that the IMPS response should depend on the photovoltage. By contrast, the IMPS response in the absence of *RC* attenuation is expected to be independent of the photovoltage if electron collection is diffusion controlled (this corresponds to a constant dc photocurrent) and if both D and τ are voltage independent (trap-free case) The theoretical treatment shows that if electron extraction is photovoltage dependent, the IMPS response should exhibit a transition from mixed diffusion/recombination control under short circuit conditions to pure recombination control as V approaches V_{oc}.

If we assume that the symmetry factor $\beta = 0.5$, eq 4a indicates that k_{ext} will decrease by a factor of 10 for a change in V_{photo} of 118 mV at 25° C. Figure 5 illustrates the effect on the IMPS signature of reducing k_{ext}. It can be seen that as a consequence of the transition from diffusion control (high k_{ext}) to recombination control (low k_{ext}), the IMPS response becomes more perfectly semicircular, and the frequency of the minimum tends toward the limit $\omega_{min} = 1/\tau$. An example of the predicted changes in ω_{min} and $\Phi_{\omega=0}$ as a function of k_{ext} is shown in Figure 6.

The IMPS plots illustrated in Figures 2−5 have been calculated for the case where *RC* attenuation is negligible. In fact, the influence of *RC* attenuation is evident even under short circuit conditions. Figure 7 shows how *RC* attenuation alters the shape of the IMPS plot under diffusion-limited extraction conditions (large k_{ext}). In the limit of high capacitance, the IMPS response becomes semicircular and is dominated by the *RC* time constant. Since the capacitance of the TiO_2 nanoc-

rystalline electrode increases as the voltage moves toward V_{oc}, *RC* attenuation may obscure the transition in the minimum frequency predicted for the case of kinetically limited electron extraction (cf. Figure 6).

Experimental Section

Dye-sensitized TiO_2 cells were prepared following the methods described by Nazeeruddin et al.[3] The electrolyte was composed of methylhexylimidazolium iodide (MHImI), iodine, 4 *tert*-butylpyridine, and acetonitrile in different concentrations. MHImI was prepared according to the method given by Papageorgiou et al.[13] Iodine was purchased from Fluka and used without further purification. Acetonitrile and *tert*-butylpyridine were purchased from Fluka and distilled under nitrogen before use.

Nanoporous TiO_2 layers were prepared from a colloidal TiO_2 dispersion obtained by hydrolysis of titanium isopropoxide. The preparation method of O'Regan and Grätzel[2] was modified to yield only the anatase modification. To obtain screen-printable pastes, the colloidal dispersions were dried and the powders ground with pine oil until a smooth dispersion was obtained. Screen printing on glass (TEC 8, fluorine doped SnO_2 on 3 mm float glass purchased from Libby Owens Ford) and subsequent firing at 450° C yielded TiO_2 layers with thicknesses of the order of 5−15 μm. These were dipped in a 3×10^{-4} M solution of the ruthenium dye cis-di(thiocyanato)-*N*,*N*-bis(2,2′-dicarboxylate)ruthenium(II) in ethanol for 2 h. The dye loading was determined to be 7.5×10^{-5} mol/g TiO_2, corresponding to 1.05×10^{-7} mol cm^{-2} (geometric) for a 12 μm film. Since the molar extinction coefficient of the dye is 4000 at 460 nm, the absorption coefficient ignoring the effects of light scattering is 800 cm^{-1}. However, transmission measurements suggest that the effective optical path length at 460 nm is at least three times greater than the film thickness, so that the effective absorption coefficient is of the order of 2500 cm^{-1}. A sandwich cell was prepared with a second conductive glass plate coated with sputter-deposited Pt (150 nm), and both plates were glued together with a transparent polyethylene (PE) hot melt. Electrolyte was introduced through holes drilled in the back electrode, and these were subsequently sealed with microscope cover plates and PE hot melt.

For the experiments with illumination from the electrolyte side, the platinum-coated electrode was replaced with a tin oxide coated electrode on which a transparent film of platinum was deposited by thermal decomposition (400° C) of a 5×10^{-3} mol dm^{-3} solution of choroplatinic acid in 2-propanol.

IMPS measurements were carried out using a combination of low-intensity modulated illumination from a blue LED (λ_{max} 460 nm) and constant white light illumination from a tungsten lamp, attenuated if necessary by Schott NG neutral density filters. The voltage across the cell was controlled by a fast operational amplifier potentiostat operating in two electrode mode. The dc $i-V$ characteristics were recorded using a voltage scan. IMPS measurements were performed using a Solartron 1250 frequency response analyzer to drive the LED and to analyze the photocurrent response. Typically the modulated intensity was at least 10^3 times smaller than the dc illumination level.

Results and Discussion

The monochromatic photocurrent conversion efficiency $\Phi = j_{photo}/qI_0$ (uncorrected for reflection losses) of the cells was determined independently in two laboratories over the wavelength range 350−850 nm (illumination from the substrate side). Broad spectra were observed with maximum values of Φ in the range 55−65% (uncorrected for reflection losses). Comparison of the photocurrent quantum efficiency with and without the reflecting platinum counter electrode indicated that reflection increased the quantum efficiency at 460 nm by less than 5%. Correction for reflection losses at the glass interface and comparison of the photocurrent action spectrum with the transmission spectrum revealed that the quantum efficiency for photocurrent generation was close to 90%.

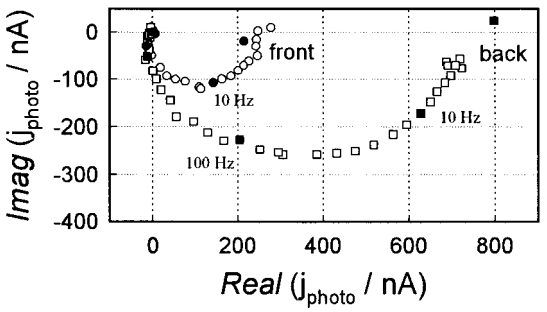

Figure 8. Comparison of experimental IMPS responses measured for illumination from the substrate side (back: $i_{sc} = 0.66$ mA) and from the electrolyte side (front: $i_{sc} = 0.25$ mA). Illumination, white light (NG 11 filter) + blue LED.

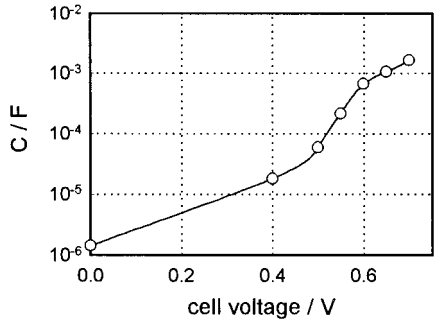

Figure 9. Capacitance of the dye-sensitized cell as a function of cell voltage (measured in the dark by electrochemical impedance spectroscopy). Note the large increase in capacitance due to electron accumulation in the nanocrystalline TiO_2 as the potential approaches flatband.

Figure 8 contrasts the short circuit IMPS responses obtained for illumination from the substrate and electrolyte sides. The shape for illumination from the substrate side is similar that reported by Cao et al.[7] The deviation from the limiting high-frequency line (cf. Figure 2) is expected for expected for *RC* attenuation (cf. Figure 7). Impedance analysis of the cells in the dark[14] showed that the series resistance is typically 8−10 Ω and the capacitance measured in the dark increases with voltage from a few microfarads at short circuit to more than 1 mF close to V_{oc} as shown in Figure 9. It was found that the most satisfactory fitting method is to use Bode plots rather than complex plane plots in order to avoid unnecessary data compression (the fitting of the phase angle plot is particularly sensitive to the choice of electron lifetime and diffusion coefficient). Figure 10 provides an example of how the magnitude and phase data from the IMPS response can be fitted satisfactorily by including the *RC* attenuation. The upper solid curve in both plots is the IMPS response in the absence of *RC* attenuation. The limiting high-frequency behavior corresponds to a slope of −0.5 in the magnitude plot and −45° in the phase plot. The addition of *RC* attenuation produces the lower solid curves that fit the data well, giving values of $\tau = 20$ ms and $D = 5 \times 10^{-5}$ cm^2 s^{-1}. It can be seen that the phase angle exceeds −90°, which indicates that the response crosses the imaginary axis at high frequencies as observed experimentally. The diffusion coefficient is of the same order of magnitude as the value determined by Solbrand et al.[17] from time-resolved

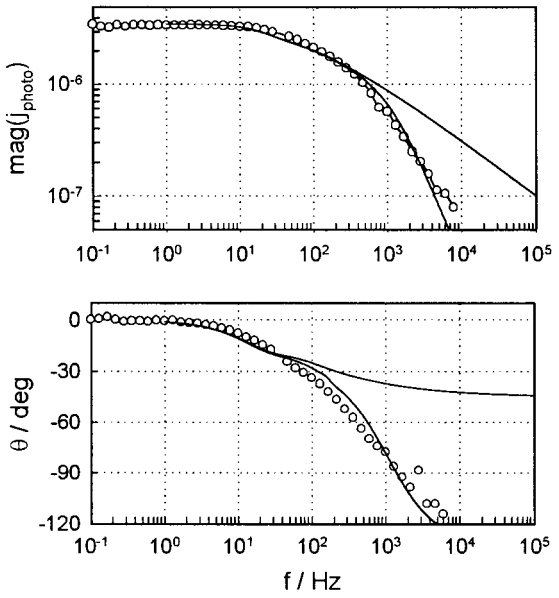

Figure 10. Bode plots of short circuit IMPS response (open circles). $i_{sc} = 6.4$ mA. The upper solid line in each plot shows the response in the absence of RC attenuation. Note the limiting high-frequency phase shift is 45°, which is characteristic for diffusion control. The lower line is the fit including *RC* attenuation. Fit parameters: $D = 5 \times 10^{-5}$ cm^2 s^{-1}, $\tau = 2 \times 10^{-2}$ s. $R = 10\ \Omega$, $C = 5 \times 10^{-5}$ F, $k_{ext} = 2.5 \times 10^4$ cm s^{-1} (diffusion controlled).

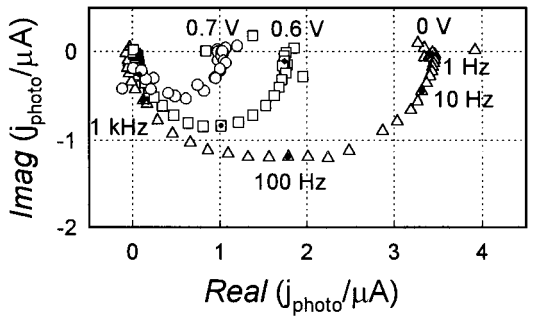

Figure 11. Potential dependence of the experimental IMPS response (illumination from substrate side: $i_{sc} = 6.14$ mA). Note that the modulated photocurrent is 3 orders of magnitude smaller than the dc photocurrent.

photocurrents for 0.7 M $LiClO_4$/ethanol but several orders of magnitude lower than the diffusion coefficient of free electrons in bulk anatase.[16,18] The capacitance obtained from the fit is 50 μF, which is more than an order of magnitude higher than the value measured by electrochemical impedance spectroscopy in the dark, indicating that accumulation occurs in the TiO_2 film under illumination at short circuit.

Measurements performed using positive feedback *iR* compensation showed that the deformation of the IMPS plot by *RC* attenuation could be reduced but not eliminated entirely. The main difficulty is that resistance is distributed across the tin oxide sheet, giving rise to a transmission line (this effect is also seen for conducting polymer films deposited on tin oxide coated glass and has been modeled elsewhere[15]).

Figure 11 illustrates a typical set of IMPS responses for illumination from the substrate side obtained at different points along the $i-V$ curve. It can be seen that the shape of the IMPS response changes as the system moves from short circuit conditions along the $i-V$ curve toward open circuit. As the dc current decreases, the low-frequency IMPS intercept also becomes smaller, the responses become progressively more semicircular, and ω_{min} decreases by a factor of 10. Interpretation of the potential dependence of ω_{min} is not straightforward since

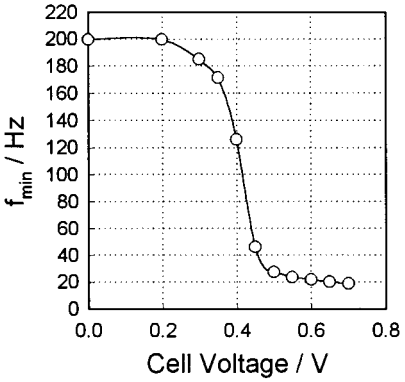

Figure 12. Potential dependence of f_{min}.

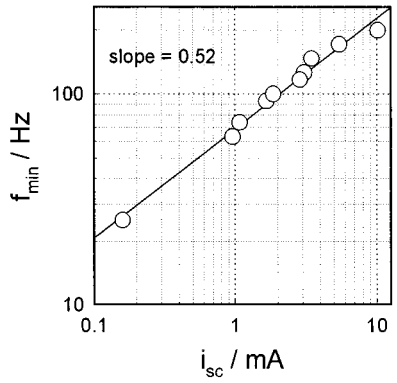

Figure 13. Intensity dependence of f_{min} measured under short circuit conditions. The short circuit current i_{sc} has been used as a linear measure of light intensity. Illumination white light + blue LED.

in principle both D and τ may be voltage dependent and hence influence ω_{min}. In fact, the change in ω_{min} shown in Figure 12 is almost certainly dominated by the increase in the *RC* time constant with potential calculated from the capacitance data shown in Figure 9, but the decrease in the zero frequency intercept indicates that either the generation[6] or the collection of electrons becomes less efficient as the potential approaches V_{oc}. Both effects are important, but *RC* attenuation begins to dominate the IMPS response in the region where kinetic limitation of electron extraction is expected to become evident in the IMPS responses.

The value of ω_{min} under short circuit conditions varies approximately with the square root of the light intensity. The log−log plot of ω_{min} vs short circuit current in Figure 13 corresponds to the power law dependence that has been reported previously by Cao et al.[7] and attributed to intensity-dependent trap filling. By contrast, measurements performed over the same intensity range at voltages close to V_{oc} showed clearly that ω_{min} becomes independent of intensity as the open circuit condition is approached.

In the case of simple diffusion control, the dc photocurrent (i.e., the difference between the current under illumination and in the dark) is expected to be independent of the voltage, unless back-reaction with the oxidized state of the dye becomes important close to V_{oc}. By contrast, the kinetic extraction model predicts that the photocurrent will decrease toward zero as the voltage is increased. Figure 14 shows that the experimental dc photocurrent does indeed decrease, and this could indicate kinetically controlled electron extraction. The experimental curve is compared in the figure with the photocurrent voltage characteristic calculated assuming $\beta = 0.5$ (see below). The fit shown is for $D = 5 \times 10^{-5}$ cm^2 s^{-1}, $\tau = 20$ ms and, k_{ext} at short circuit $= 2.5 \times 10^4$ cm s^{-1}. However, the decrease in photocurrent may reflect the increasing rate of back-reaction

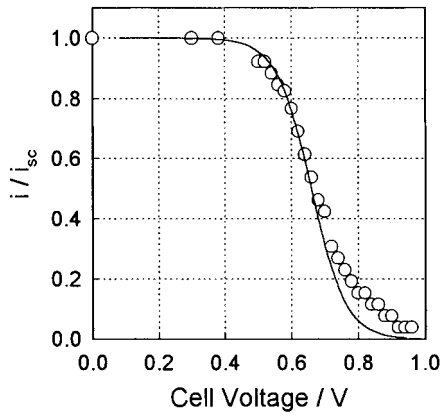

Figure 14. Normalized steady-state photocurrent voltage characteristic. Illumination from substrate side: i_{sc} 5.2 mA. The line shows the best fit of the data to eq 9 (k_{ext} (at $V = 0$) 2.5×10^4 cm s^{-1}, $D = 5 \times 10^{-5}$ cm^2 s^{-1}, $\tau = 2.0 \times 10^{-2}$ s, $d = 12$ μm, $\alpha = 2500$.

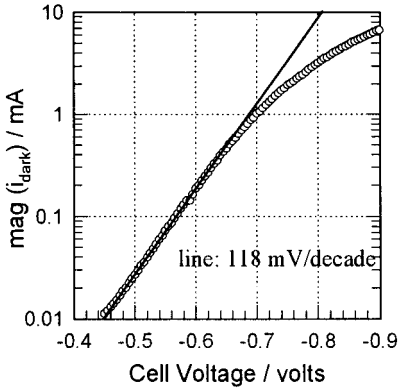

Figure 15. Semilogarithmic plot of the dark current−voltage characteristic. The slope corresponding to $\beta = 0.5$ in eq 4a is shown. Note that this corresponds to a diode ideality factor $m = 2$ in eq 2.

of electrons with the oxidized state of the dye[6] or possibly the voltage dependence of D and τ. To distinguish between these possibilities it would be necessary to eliminate the effect of the *RC* time constant on the IMPS response.

The dark current voltage characteristics of the cells were measured in order to determine the diode ideality factor (m in eq 2). Figure 15 shows that the slope of the semilogarithmic plot is 118 mV/decade, which corresponds to the value $m = 2$ reported by other authors.[4,5] This value corresponds to $\beta = 0.5$ in eq 4b, which describes electron injection from the substrate into the TiO_2 film. At higher current densities, the plot flattens, suggesting that diffusion control and ohmic losses become important. The potential drop at the TiO_2/electrolyte interface will also vary under strong electron accumulation. The dark-current characteristic supports the conclusion that the rate of electron transfer at the substrate/TiO_2 interface is voltage dependent.

Conclusions

The theoretical treatment of electron collection, recombination, and extraction in the nanocrystalline dye-sensitized cell successfully predicts the features of the observed IMPS responses. The electron diffusion coefficient derived from the IMPS analysis is nearly 4 orders of magnitude lower than values estimated from the room-temperature Hall mobilities reported for electrons in sputtered thin films[16] and single-crystal[18] anatase, indicating that electron transport in the porous layer is much slower than in the bulk phase. Further work is needed to develop models for charge transport and trapping in the nanocrystalline phase, but the present results show that the use of effective diffusion coefficients and electron lifetimes remains valid as long as electron trapping and detrapping occur on a time scale that is short compared with the light perturbation. The experimental results confirm all the main predictions of the model, and they provide information about the characteristics of the high-efficiency cells that are currently being developed. IMPS should be a useful method for the optimization of cell design. In principle, the IMPS response can be related to the time-resolved photocurrent response[17] and to the frequency-resolved photovoltage response. Further work on these aspects is in progress.

Acknowledgment. We thank Professor Grätzel and members of his group for close and fruitful cooperation and the Ministry of the Economy of Nordrhein-Weststfalen (Germany) for financial support. N.J.S. acknowledges support in the form of a Clean Technology studentship from the U.K. Engineering and Physical Science Council. This work was also supported by the University of Bath.

Appendix

A1. The Trap Free Case. We consider the general case where the rate of electron extraction is characterized by a first-order heterogeneous rate constant k_{ext}. The ac component of the illumination is of the form

$$I(t) = I_0 e^{i\omega t} \tag{A1}$$

For illumination from the substrate side, the diffusion equation for the excess electron concentration, n, in the absence of trapping effects is given by

$$\frac{\partial n}{\partial t} = D\frac{\partial^2 n}{\partial x^2} - \frac{n}{\tau} + \alpha I_0 e^{-\alpha x} e^{i\omega t} \tag{A2}$$

where D is the effective diffusion coefficient of electrons, d is the film thickness, x is the distance from the substrate, and τ is the pseudo-first-order electron lifetime determined by recombination with I_3^-.

The boundary conditions are

$$k_{ext} n(0,t) = D\frac{\partial n}{\partial x}|_{x=0} \tag{A3}$$

$$\frac{\partial n(x,t)}{\partial x}|_{x=d} = 0 \tag{A4}$$

The time-dependent electron concentration will be of the form

$$n(x,t) = u(x) e^{i\omega t} \tag{A5}$$

so that the equations transform into

$$u'' = u\left(\frac{1}{D\tau} + \frac{i\omega}{D}\right) - \alpha\frac{I_0}{D} e^{-\alpha x} \tag{A6}$$

with the boundary conditions

$$u'(d) = 0 \tag{A7}$$

$$Du'(0) = k_{ext} u(0) \tag{A8}$$

The solution takes the form

$$u(x) = Ae^{\gamma x} + Be^{-\gamma x} + Ce^{-\alpha x} \tag{A9}$$

where

$$\gamma = \sqrt{\left(\frac{1}{D\tau} + \frac{i\omega}{D}\right)} \tag{A10}$$

The coefficients *A*, *B*, and *C* can be evaluated from eqs A6−A9

$$C = \frac{\alpha I_0/D}{\gamma^2 - \alpha^2} \tag{A11}$$

$$A = C\,\frac{\alpha e^{-\alpha d}(k_{ext} + \gamma D) - \gamma e^{-\gamma d}(k_{ext} + \alpha D)}{\gamma(k_{ext}(e^{\gamma d} + e^{-\gamma d}) + D\gamma(e^{\gamma d} - e^{-\gamma d}))} \tag{A12}$$

$$B = -C\,\frac{\alpha e^{-\alpha d}(k_{ext} + \gamma D) + \gamma e^{\gamma d}(k_{ext} + \alpha D)}{\gamma(k_{ext}(e^{\gamma d} + e^{-\gamma d}) + D\gamma(e^{\gamma d} - e^{-\gamma d}))} \tag{A13}$$

The ac component of the photocurrent is

$$j(\omega) = D\left(\frac{\partial u}{\partial x}\right)|_{x=0} = D(A\gamma - B\gamma - C\alpha) \tag{A14}$$

The ac photocurrent conversion efficiency $\Phi(\omega)$ then takes the final form

$$\Phi(\omega) = \frac{\alpha}{\alpha + \gamma} \cdot \frac{e^{\gamma d} - e^{-\gamma d} + 2\alpha\,\dfrac{e^{-\alpha d} - e^{-\gamma d}}{\gamma - \alpha}}{e^{\gamma d} + e^{-\gamma d} + \dfrac{D\gamma}{k_{ext}}(e^{\gamma d} - e^{-\gamma d})} \tag{A15}$$

An analogous treatment for illumination from the electrolyte side with appropriate boundary condition gives

$$u(x) = Ae^{\gamma x} + Be^{-\gamma x} + Ce^{\alpha x} \tag{A9a}$$

$$C = \frac{\alpha I_0/D}{\gamma^2 - \alpha^2}\,e^{-\alpha d} \tag{A11a}$$

$$A = -C\,\frac{\alpha e^{-\alpha d}(k_{ext} + \gamma D) + \gamma e^{-\gamma d}(k_{ext} - \alpha D)}{\gamma(k_{ext}(e^{\gamma d} + e^{-\gamma d}) + D\gamma(e^{\gamma d} - e^{-\gamma d}))} \tag{A12a}$$

$$B = C\,\frac{\alpha e^{-\alpha d}(k_{ext} + \gamma D) + \gamma e^{\gamma d}(\alpha D - k_{ext})}{\gamma(k_{ext}(e^{\gamma d} + e^{-\gamma d}) + D\gamma(e^{\gamma d} - e^{-\gamma d}))} \tag{A13a}$$

$$\Phi(\omega) = \frac{\alpha}{\alpha + \gamma} \cdot \frac{e^{(\gamma-\alpha)d} - e^{-(\alpha+\gamma)d} + 2\alpha\,\dfrac{e^{(\gamma-\alpha)d} - 1}{\gamma - \alpha}}{e^{\gamma d} + e^{-\gamma d} + \dfrac{D\gamma}{k_{ext}}(e^{\gamma d} - e^{-\gamma d})} \tag{A16}$$

The corresponding concentration profile is obtained from eqs A9−A13 by setting

$$\gamma = \sqrt{\left(\frac{1}{D\tau}\right)} \tag{A17}$$

Similarly the dc photocurrent is obtained from eq A15 and A16 by making the same substitution.

For a certain set of parameters and $\omega = 0$ it may happen that $\alpha = \gamma$. For this special case, the dc conversion efficiency is

$$\Phi(\omega{=}0) = \frac{\dfrac{e^{\gamma d} - e^{-\gamma d}}{2} + \gamma d e^{-\alpha\gamma d}}{e^{\gamma d} + e^{-\gamma d} + \dfrac{D\gamma}{k_{ext}}(e^{\gamma d} - e^{-\gamma d})} \tag{A18}$$

for illumination from the substrate side and

$$\Phi(\omega{=}0) = \frac{\dfrac{1 - e^{-2\gamma d}}{2} + \gamma d}{e^{\gamma d} + e^{-\gamma d} + \dfrac{D\gamma}{k_{ext}}(e^{\gamma d} - e^{-\gamma d})} \tag{A19}$$

for the illumination from the electrolyte side.

A2. The Influence of Electron Trapping. We restrict ourselves to the diffusion case and illumination from the substrate side. Electrons are trapped with a first-order rate constant k_{trap} that depends on the thermal velocity of electrons as well as the capture cross section, density, and occupation of traps (in general k_{trap} is expected to decrease as electron traps are filled progressively by increasing the illumination intensity). The rate of release of electrons from traps is characterized by a first-order rate constant k_{detrap} that is determined by the trap depth and the temperature. In principle k_{trap} may be distance-dependent due to the variation of the electron quasi-Fermi level. However, here we assume that both k_{trap} and k_{detrap} are constant throughout the film in order to obtain a simple analytical solution that provides a diagnostic test for trapping effects.

The diffusion equation for electrons in the conduction band (for illumination from the substrate side) becomes

$$\frac{\partial n}{\partial t} = D\,\frac{\partial^2 n}{\partial x^2} - \frac{n}{\tau_{cb}} - k_1 n + k_2 N + \alpha I_0 e^{-\alpha x} \cdot e^{i\omega t} \tag{A20}$$

Here N is the density of trapped electrons and τ_{cb} is the lifetime for recombination of free electrons with I_3^-.

The density of trapped electrons is given by

$$\frac{\partial N}{\partial t} = k_{trap} n - k_{detrap} N - \frac{N}{\tau_{trap}} \tag{A21}$$

Here τ_{trap} is the lifetime for recombination of trapped electrons with I_3^-.

The solution takes the same forms as that obtained in the absence of trapping, except that γ (cf. eq A10) is now given by

$$\gamma^2 = \frac{1}{D\tau_{cb}} + \frac{k_{trap}}{D}\,\frac{\dfrac{1}{\tau_{trap}}\left(k_{detrap} + \dfrac{1}{\tau_{trap}}\right) + \omega^2}{\left(k_{detrap} + \dfrac{1}{\tau_{trap}}\right)^2 + \omega^2} + i\frac{\omega}{D}\left(1 + \frac{k_{trap}k_{detrap}}{\left(k_{detrap} + \dfrac{1}{\tau_{trap}}\right)^2 + \omega^2}\right) \tag{A22}$$

If k_{trap} and $k_{detrap} \gg \omega$, then we recover the original expressions with the effective electron lifetime τ_{eff} and effective diffusion coefficient D_{eff} defined by

$$\frac{1}{\tau_{eff}} = \frac{1}{\tau_{cb}} + \frac{k_{trap}}{1 + k_{detrap}\tau_{trap}} \tag{A23}$$

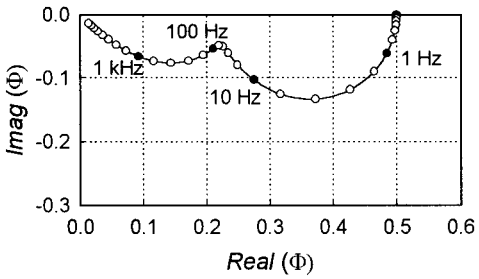

Figure 16. IMPS characteristic calculated for the case where trapping/detrapping occurs on a time scale comparable to measurement frequencies. $D = 10^{-4}$ cm^2 s^{-1}, $\tau_{cb} = 10^{-2}$ s, $\tau_{trap} = \infty$, $\alpha = 10^4$ cm^2 s^{-1}, $k_{trap} = 10^3$ s^{-1}, $k_{detrap} = 100$ s^{-1}.

and

$$D_{eff} = \frac{D}{1 + \frac{k_{trap}k_{detrap}}{\left(k_{detrap} + \frac{1}{\tau_{trap}}\right)^2}} \qquad \text{(A24)}$$

These expressions show that trapping increases the recombination rate of electrons and decreases their effective diffusion coefficient.

This analysis shows that the effects of trapping are not distinguishable unless the rate constants k_{trap} and k_{detrap} are comparable with the modulation frequency ω, in which case the IMPS response resolves into two parts as illustrated by Figure 16. To simplify the diagnostic value of the plot, it has been assumed that no recombination of trapped electrons occurs.

References and Notes

(1) Vlachopoulos, N.; Liska. P.; Augustynski, J.; Grätzel, M. *J. Am. Chem. Soc.* **1988**, *110*, 1216.

(2) O'Regan. B; Grätzel, M. *Nature* **1991**, *353*, 737.

(3) Nazeeruddin, M. K.; Kay, A.; Rodicio, I.; Humphry-Baker, R.; Müller, E.; Liska, P.; Vlachopoulos, N.; Grätzel, M. *J. Am. Chem. Soc.* **1993**, *115*, 6382.

(4) Södergren, S.; Hagfeldt, A.; Olsson, J.; S.-E. Lindquist, S. E. *J. Phys. Chem.* **1994**, *95*, 5522.

(5) Huang, S. Y.; Schlichthörl, G.; Nozik, A. J.; Grätzel, M.; Frank, A. J. *J. Phys. Chem. B* **1997**, *101*, 2576.

(6) O'Regan, B.; Moser, J.; Anderson, M.; Grätzel, M. *J. Phys.Chem.* **1990**, *94*, 8720.

(7) Cao, F.; Oskam, G.; Meyer, G. J.; Searson, P. C. *J. Phys. Chem.* **1996**, *100*, 17021.

(8) de Jongh, P. E.; Vanmaekelbergh, D. *Phys. Rev. Lett.* **1996**, *77*, 3427.

(9) de Jongh, P. E; Vanmaekelbergh, D. *J. Phys. Chem. B* **1997**, *101*, 2716.

(10) Vanmaekelbergh, D.; Iranzo Marín, F.; van de Lagemaat, J. *Ber. Bunsen-Ges. Phys. Chem.* **1996**, *100*, 616.

(11) Schwarzburg K.; Willig, F. *Appl. Phys. Lett.* **1991**, *58*, 2520.

(12) Peter, L. M. *Chem Rev.* **1990**, *90*, 753.

(13) Papageorgiu, N.; Athanassov, Y.; Armand, M.; Bonhote, P.; Petterson. H.; Azam, A.; Grätzel, M. *J. Am. Chem. Soc.* **1993**, *143*, 3099.

(14) Dloczik, I.; Lauermann, I; Peter, L. M.; Ponomarev, E. A.; Shaw, N. J.; Uhlendorf, I., in preparation.

(15) Kalaji, M.; Peter, L. M. *R. Soc. Chem. Faraday Trans.* **1991**, *87*, 853.

(16) Tang, H.; Prasad, K.; Sanjinès, R.; Schmid, P. E.; Lévy F. *J. Appl. Phys.* **1995**, *75*, 2042.

(17) Solbrand, A.; Lindström, H.; Rensmo H.; Hagfeldt A.; Lindquist, S. E.; Södergren, S. *J. Phys. Chem. B* **1997**, 101, 2514.

(18) Forro, L.; Chauvet, O.; Emin, D.; Zuppiroli, L.; Berger, H.; Lévy, F. *J. Appl. Phys.* **1994**, *75*, 633.